

## Optical Entanglement of Distinguishable Quantum Emitters

D. S. Levonian<sup>1,2</sup>, R. Riedinger<sup>1,3,4</sup>, B. Machielse<sup>1,2</sup>, E. N. Knall<sup>5</sup>, M. K. Bhaskar<sup>1,2</sup>, C. M. Knaut<sup>1</sup>, R. Bekenstein,<sup>1,6</sup>  
H. Park,<sup>1,7</sup> M. Lončar,<sup>5</sup> and M. D. Lukin<sup>1,\*</sup>

<sup>1</sup>*Department of Physics, Harvard University, Cambridge, Massachusetts 02138, USA*

<sup>2</sup>*AWS Center for Quantum Computing, Pasadena, California 91125, USA*


<sup>3</sup>*Institut für Laserphysik und Zentrum für Optische Quantentechnologien, Universität Hamburg, 22761 Hamburg, Germany*

<sup>4</sup>*The Hamburg Centre for Ultrafast Imaging, 22761 Hamburg, Germany*

<sup>5</sup>*John A. Paulson School of Engineering and Applied Sciences, Harvard University, Cambridge, Massachusetts 02138, USA*

<sup>6</sup>*Racah Institute of Physics, The Hebrew University of Jerusalem, Jerusalem 91904, Israel*

<sup>7</sup>*Department of Chemistry and Chemical Biology, Harvard University, Cambridge, Massachusetts 02138, USA*

 (Received 23 August 2021; accepted 21 March 2022; published 23 May 2022)

Solid-state quantum emitters are promising candidates for the realization of quantum networks, owing to their long-lived spin memories, high-fidelity local operations, and optical connectivity for long-range entanglement. However, due to differences in local environment, solid-state emitters typically feature a range of distinct transition frequencies, which makes it challenging to create optically mediated entanglement between arbitrary emitter pairs. We propose and demonstrate an efficient method for entangling emitters with optical transitions separated by many linewidths. In our approach, electro-optic modulators enable a single photon to herald a parity measurement on a pair of spin qubits. We experimentally demonstrate the protocol using two silicon-vacancy centers in a diamond nanophotonic cavity, with optical transitions separated by 7.4 GHz. Working with distinguishable emitters allows for individual qubit addressing and readout, enabling parallel control and entanglement of both colocated and spatially separated emitters, a key step toward scaling up quantum information processing systems.

DOI: [10.1103/PhysRevLett.128.213602](https://doi.org/10.1103/PhysRevLett.128.213602)

Solid-state quantum emitters have recently emerged as promising candidates for the realization of quantum networks. They combine a number of advantageous properties including electronic spin qubits with long coherence times [1–3], fast gates [4], access to nuclear qubit registers [5,6], deterministic qubit fabrication [7–9], and accessible operating temperatures [6,10]. The most important challenge in scalable quantum information processing with defect centers involves generating high-fidelity entanglement between spatially separated defects.

Entanglement mediated by photons stands out in comparison with other promising approaches [11–13] as a unique mechanism for long distance entanglement even across room-temperature environments [14]. Long distance entanglement can be used for quantum repeaters and the creation of quantum networks [15–17]. Fast and efficient spin-photon gates in solid-state emitters were recently demonstrated by employing cavity quantum electrodynamics (CQED), with integration of color centers in nanophotonic resonators enabling reproducible, compact, on-chip architectures [4]. These advances enabled the demonstration of Bell state measurements on asynchronously arriving photons [18], a key capability of quantum repeater stations.

Despite the rapid progress in this area [19], the state-of-the-art photonic entanglement schemes are incompatible

with the broad distribution of optical transitions commonly exhibited by solid-state emitters due to strain variations. Using frequency-erasing time-tagging or electro-optical frequency shifting, entanglement of distinguishable memories separated by at most  $\sim 100$  MHz has been demonstrated [20,21], which falls short of the typical frequency spread of  $\sim 5$ –150 GHz for emitters encountered in micro- and nanophotonic structures [8,22,23]. While multistage quantum frequency conversion could cover this mismatch, its high noise and low efficiency have so far restricted its application to conversion from emitter wavelengths to telecommunication wavelengths for long distance communication [24–26]. Instead, individual quantum emitters with near-identical optical resonances are postselected [27–29], or the optical detuning is actively compensated [14,30]. In practice, however, such schemes have limited scalability, the former due to its low yield, and the latter due to substantial overhead in device complexity.

In this Letter, we propose and demonstrate a scheme to entangle emitters with far-detuned optical transitions which are coupled to an optical cavity. We experimentally realize it using two silicon-vacancy color centers (SiV) in the same diamond photonic crystal resonator, each acting as a spin-dependent scatterer. Our scheme [illustrated in Figs. 1(a)–1(c)] is inspired by the Elitzur-Vaidman Gedanken experiment [31]. Embedding the two SiVs in

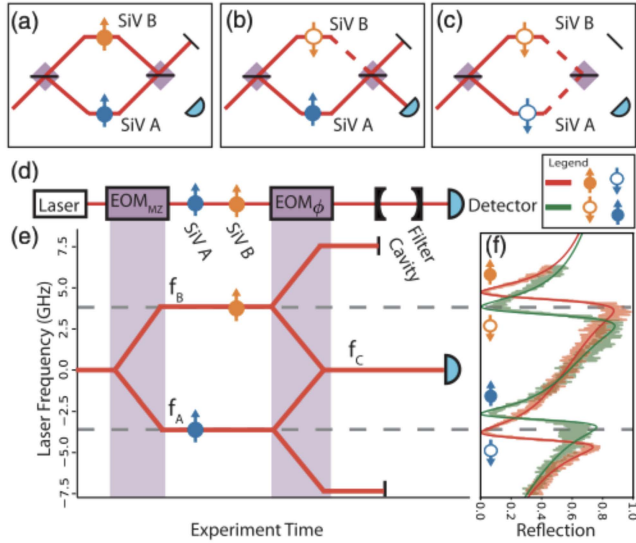


FIG. 1. Optical entanglement of distinguishable emitters. (a) An interferometer is tuned so that when no spin scatters light (full circle) photons leave only through the top port of the interferometer. (b) If just one spin scatters (empty circle) while the other reflects, light is split between the two output ports, and the heralding detector receives photons. (c) If both spins scatter, no light leaves the interferometer. (d) The physical implementation of the protocol. The two SiVs act as spin-dependent mirrors. The relative phase between the microwave drive to the two modulators  $\text{EOM}_{MZ}$  and  $\text{EOM}_{\phi}$  sets the phase difference between the interferometer arms. (e) The Elitzur-Vaidman Gedanken experiment implemented as a frequency domain interferometer. The y axis shows the relative frequency of the relevant photonic modes in the protocol. Two EOMs (purple) play the role of beam splitters. Detection of photons at the central frequency projects the SiVs into an odd parity state. (f) The spectrum of the two SiVs under investigation, when initialized in  $|\uparrow\downarrow\rangle$  (green) or  $|\downarrow\uparrow\rangle$  (red).

the two arms of an interferometer, we use an interaction-free measurement to determine if one (and only one) arm is blocked, determining the joint spin parity by monitoring a dark port of the interferometer [32,33]. Unlike the original scheme (and proposed applications to qubit entanglement [34]), our approach uses a frequency-domain interferometer [see Figs. 1(d) and 1(e)], allowing a single heralding photon to entangle quantum emitters with drastically different optical transition frequencies.

The implementation is illustrated in Figs. 1(d) and 1(e). SiV centers  $A$  and  $B$  are detuned from the nanophotonic cavity such that the system exhibits spin-dependent spectral features of high contrast due to differential Zeeman splitting of the ground and excited states. The optical transition of SiV  $A$  ( $B$ ) is only resonant with frequency  $f_A$  ( $f_B$ ), if the spin is in the  $|\downarrow\rangle_{A(B)}$  state, which results in photons being scattered and lost from the interferometer. Otherwise (for  $|\uparrow\rangle_{A(B)}$ ), a Fano interference blocks the light from entering the cavity [Fig. 1(f), Ref. [4]], keeping it in the interferometer.

In each round, the spins of SiVs  $A$  and  $B$  are first initialized in the state

$$|-\rangle_A \otimes |+\rangle_B \propto |\uparrow\uparrow\rangle_{AB} + |\uparrow\downarrow\rangle_{AB} - |\downarrow\uparrow\rangle_{AB} - |\downarrow\downarrow\rangle_{AB}, \quad (1)$$

with  $|\pm\rangle_{A(B)} = (|\uparrow\rangle_{A(B)} \pm |\downarrow\rangle_{A(B)})/\sqrt{2}$  [35], and a photon is prepared in a superposition of two frequency-domain basis states  $|f_A\rangle$  and  $|f_B\rangle$ :

$$|\psi\rangle_{p,\text{in}} = \frac{1}{\sqrt{2}}(|f_A\rangle_{p,\text{in}} + |f_B\rangle_{p,\text{in}}). \quad (2)$$

This is achieved by sending a photon at frequency  $f_C = (f_A + f_B)/2$  through an electro-optic amplitude modulator ( $\text{EOM}_{MZ}$ ) driven at  $\omega = (f_B - f_A)/2$  to produce two sidebands at  $f_A$  and  $f_B$  while suppressing the carrier. The photon then encounters the two SiVs, where each frequency component is conditionally reflected into the modes described by annihilation operators  $\hat{a}$  (for  $f_A$ ) and  $\hat{b}$  (for  $f_B$ ). Next, the two sidebands are recombined, using a phase modulator ( $\text{EOM}_{\phi}$ ), yielding the mode described by  $\hat{c} = (1/\sqrt{2})(e^{i\Delta\phi}\hat{a} + \hat{b})$  at frequency  $f_C$  ( $\Delta\phi$  relative phase). Finally, the light is sent through a filter cavity, which rejects the sidebands, and is detected by a single photon detector [Fig. 1(d)].

In case the spins are in the  $|\uparrow\uparrow\rangle_{AB}$  state, both frequency components are reflected, such that the probe photon is in state  $|\psi\rangle_p \propto |f_A\rangle_p + |f_B\rangle_p$  when it arrives at the frequency combiner  $\text{EOM}_{\phi}$ , where  $|f_{A(B)}\rangle_p$  indicates a photon in the mode described by  $\hat{a}$  ( $\hat{b}$ ). We set the interferometer phase  $\Delta\phi = \pi$ , so that the mode at  $f_C$  becomes a dark port of the interferometer, with the amplitudes  $\hat{a}$  and  $\hat{b}$  interfering destructively. The second EOM transfers the probe photon to the modes at  $f_C \pm 2\omega$  [Fig. 1(a)], where it is rejected by the filter cavity. In case of the  $|\downarrow\downarrow\rangle_{AB}$  state, there is no photon reflection at either  $f_A$  or  $f_B$  [Fig. 1(c)], also resulting in no events at the detector. For  $|\uparrow\downarrow\rangle_{AB}$  and  $|\downarrow\uparrow\rangle_{AB}$ , only one of the frequency components is blocked, destroying the interference condition at the final frequency beam splitter and allowing the photon to pass through the interferometer [Fig. 1(b)], revealing the spin parity.

Similar to the Elitzur-Vaidman Gedanken experiment, transmission of the photon implies that it did not encounter the scatterer, but nonetheless reveals the scatterer's presence, a phenomenon termed interaction-free measurement. Importantly, an event at the heralding detector does not reveal which frequency path was blocked, as the photon could originate from either component of the spin-photon state:  $|\psi_{\text{out}}\rangle_{AB,p} \sim -|\uparrow\downarrow\rangle_{AB} \otimes |f_A\rangle_p + |\downarrow\uparrow\rangle_{AB} \otimes |f_B\rangle_p$ . A detection event in mode  $\hat{c}$  thus projects the spins to a maximally entangled Bell state:

$$|\Psi^+\rangle_{AB} = \frac{|\uparrow\downarrow\rangle_{AB} + |\downarrow\uparrow\rangle_{AB}}{\sqrt{2}} \quad (3)$$

This interferometric protocol is robust and resource efficient compared with other optical entanglement protocols. As both frequency components travel on a common path, the protocol is robust to phase fluctuations of the fiber, requiring no active stabilization of the interferometer and hence reducing the experimental overhead. At the same time, detection of a single photon is sufficient to herald entanglement, in contrast to the most widely used robust schemes, which require two photons [36].

Conventional commercial EOMs and signal generators suffice for generating entanglement between emitters separated by up to  $|f_A - f_B| \leq 80$  GHz in the visible and near infrared wavelength range. This range can be extended to 160 GHz by selecting higher order EOM sidebands with spectral filters. This covers the majority of the inhomogeneous distribution of various color centers in nanostructures, such as C:SiV<sup>-</sup>, [8], YSO:Er<sup>+3</sup> [22], and YSO:Nd<sup>+3</sup> [37].

Our experimental implementation [Fig. 2(a)] utilizes a pair of SiV<sup>-</sup> centers (*A* and *B*) with optical transitions separated by 7.4 GHz, located in the same nanophotonic cavity [4] with cooperativities  $C_A = 14.4(1)$  and  $C_B = 6.1(1)$ , respectively [19]. The cavity is coupled to a waveguide, which adiabatically transfers photons into a tapered fiber with an efficiency of  $\eta_{wg} = 0.85 \pm 0.03$ . The cavity is detuned from the SiV transitions to yield high reflection contrast for both SiV *A* and *B* [Fig. 1(f) in the Supplemental Material [38]]. A magnetic field of  $B \sim 0.45$  T is applied along the common symmetry axis of both SiVs to split the spin conserving optical transitions (with probability of spin changing transition  $r \sim 2.3 \times 10^{-4}$  per optical cycle).

To read out SiV *A* (*B*), we inject photons at frequency  $f_A$  ( $f_B$ ) and detect them with a superconducting nanowire single photon detector placed before the filter cavity [see Fig. 2(a)]. This allows for an independent readout of both spin states with fidelity  $\mathcal{F}_{R,A} = 0.9984(1)$  and  $\mathcal{F}_{R,B} = 0.9991(1)$  [38]. Moreover, the gyromagnetic ratio of SiVs depends significantly on strain, allowing for individual microwave addressing of emitters with the same orientation. Here, we find Zeeman splitting of the ground state spin states of  $\omega_{ZA} = 12.285$  GHz and  $\omega_{ZB} = 12.627$  GHz [38], allowing independent control of the individual spins.

The spins are sequentially initialized, via detection of their state and application of a local rotation to each qubit with a resonant microwave pulse to prepare the state  $|-\rangle_{AB}$ . Without optical input, we find that an interleaved Hahn-Echo sequence on both spins with pulses separated by  $\tau_1 = 412$  ns and  $\tau_2 = 423$  ns respectively [Fig. 3(a)] recovers the initial two-spin state with a fidelity of  $\mathcal{F}_{HE,AB} = 0.93$ , consistent with the corresponding individual Hahn-Echo fidelities  $\mathcal{F}_{HE,A} = 0.96$  and  $\mathcal{F}_{HE,B} = 0.97$  [47]. We note

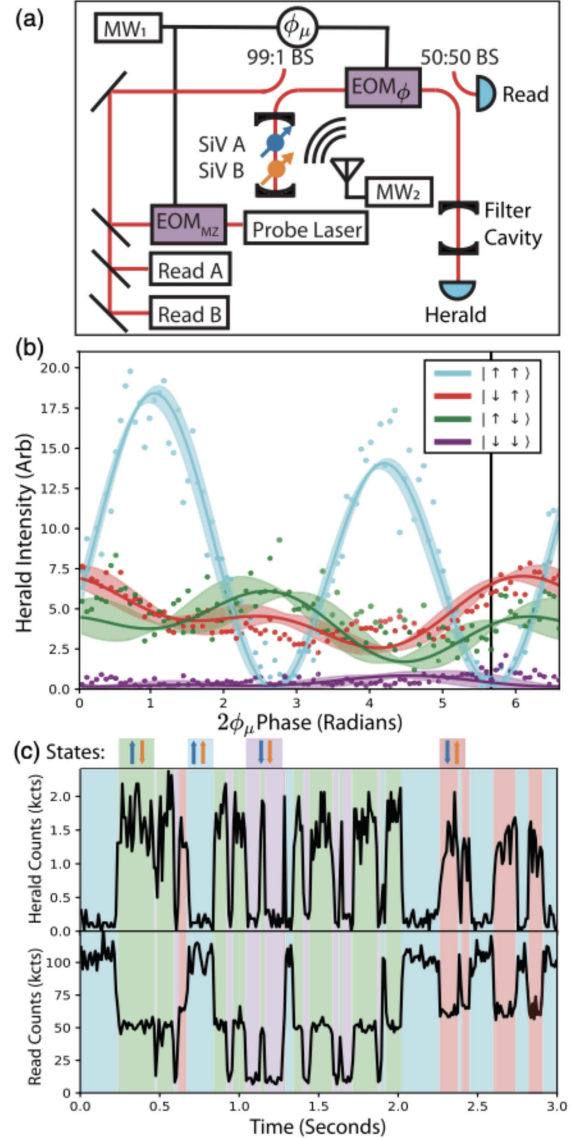


FIG. 2. (a) Detailed experimental implementation. The relative phase  $\phi_\mu$  between the microwave drive (MW<sub>1</sub>) to the two modulators EOM<sub>MZ</sub> and EOM<sub>φ</sub> sets the phase difference between the interferometer arms  $\Delta\phi = 2\phi_\mu$ . Readout is done sequentially with lasers at  $f_A$  and  $f_B$  by detecting a fraction of the light before the filter cavity. (b) Transmission to the heralding port vs interferometer phase for all SiV states  $|\downarrow\uparrow\rangle$  (red circles),  $|\uparrow\downarrow\rangle$  (green),  $|\uparrow\uparrow\rangle$  (cyan), and  $|\downarrow\downarrow\rangle$  (purple). Transmission predicted by a fit of the spin-dependent reflection spectrum [Fig 1(f)] as solid lines with variance due to spectral diffusion given by shaded area. Phase and scaling are obtained by fitting the  $|\uparrow\uparrow\rangle$  state. The black vertical line indicates the phase used to collect the entanglement data. (c) Quantum jumps. Transmission through the filter cavity (top panel) and readout port (bottom panel) vs time with the entanglement heralding laser applied continuously. The filter transmission is a spin parity measurement, with high transmission corresponding to odd parity ( $|\uparrow\downarrow\rangle$  or  $|\downarrow\uparrow\rangle$ ) highlighted with green or red background. Practically, we can distinguish these states by their slightly different transmission amplitudes through the readout port. Low transmission indicates either  $|\uparrow\uparrow\rangle$  (blue background) or  $|\downarrow\downarrow\rangle$  (purple background).

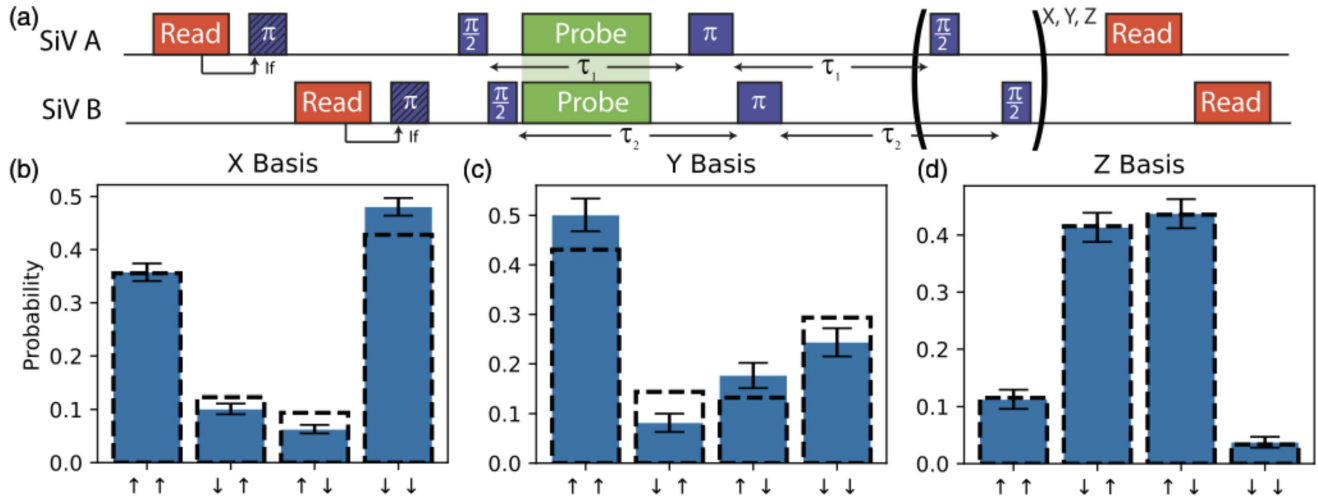


FIG. 3. (a) The schematic of the sequence used to entangle the spins. Initialization and readout both apply  $10 \mu\text{s}$  laser pulses at  $f_A$  or  $f_B$ . Counts are subsequently compared to a threshold to determine the state. Initialization follows this with a conditional  $\pi$  pulse. (b)–(d) Correlation statistics of the entangled state in  $XX$ ,  $YY$ , and  $ZZ$  spin bases. In the experimental data (blue), the measurement was taken with a heralding window of 200 ns. Dashed black lines are correlations predicted by a theoretical model. Error bars represent 68% confidence interval. Correlation data are composed of 407Z basis heralds, 913X basis heralds, and 222Y basis heralds [38].

that due to drifts in qubit frequencies, the fidelity is reduced during long measurements (resulting, e.g., in average  $\langle \mathcal{F}_{\text{HE},AB} \rangle = 0.85$  over 3 days of measurements).

We tune the phase of the frequency-bin interferometer by initializing the spins in  $|\uparrow\uparrow\rangle_{AB}$  and minimizing the transmission through the interferometer [Fig. 2(b), black line]. At the optimal phase, we find the relative transmission rates for the four spin states  $T_{\uparrow\uparrow}:T_{\uparrow\downarrow}:T_{\downarrow\uparrow}:T_{\downarrow\downarrow} = 1:14:22:1.2$ . Quantum jumps of the parity readout are shown in Fig. 2(c). The mismatch in reflection between the two odd parity states  $|\uparrow\downarrow\rangle_{AB}$  ( $|\downarrow\uparrow\rangle_{AB}$ ) is due to interference of the light reflected by the  $|\uparrow\rangle$  state by SiV A (B) with the residual reflection of the  $|\downarrow\rangle$  state of SiV B (A) and the leaked carrier at  $f_C$  and can vary depending on their relative phases. Similarly,  $T_{\downarrow\downarrow}$  is limited by interference of the finite reflection in the  $|\downarrow\rangle$  states with the leaked carrier. For  $T_{\uparrow\uparrow}$  the largest contribution to the finite reflection is the spectral diffusion of the two SiV features and the resulting fluctuation in the phase of the reflected light.

We entangle the spins by sending a weak coherent pulse with an expected photon number of 0.1 at the cavity into the interferometer, striking a balance between success probability and decoherence induced by the scattering of extra, undetected heralding photons. When a photon is detected in the transmission of the filter cavity, this heralds that the spins were prepared in an entangled state.

To characterize this state, we sequentially measure the correlations of the spins of SiV A and B in the X, Y, and Z basis (see Fig 3). This results in a measured fidelity of

$$\mathcal{F}_{|\Psi^+\rangle} = (2p_{\uparrow\downarrow} + 2p_{\downarrow\uparrow} + K_{XX} + K_{YY})/4 = 0.71(2) \quad (4)$$

where  $K_{BB} = p_{++} + p_{--} - p_{+-} - p_{-+}$  is the contrast for basis  $B = X, Y$  and  $p_{ab}$  is the probability for measuring the spin of SiV A (B) in  $a(b) \in \{+, -\}$  in the X and Y basis, respectively, and  $a(b) \in \{\uparrow, \downarrow\}$  in the Z basis. This confirms that the spins are entangled ( $\mathcal{F}_{|\Psi^+\rangle} > 0.5$ ). As an alternative measure of entanglement, we obtain a concurrence of  $\mathcal{C} \geq 0.37(4)$  [38].

To understand the limitations of our protocol and the role of imperfections, we compare our experimental results to a model based on the spectrum of the CQED system [Fig. 1(f)]. Using the complex reflection coefficient at frequencies  $f_A$ ,  $f_B$ , and  $f_C$ , we obtain a predicted transmission through the interferometer for all four spin states [Fig. 2(b)] [48]. The residual difference between the data and the model is consistent with an offset in the reflection spectrum and a nonzero relative phase of the leaked carrier at  $f_C$  [38].

Including local qubit errors and accounting for a phase drift of the carrier, our model predicts the correlations of the heralded state [see Figs. 3(b)–3(d)], and a fidelity of  $\sim 0.67 \pm 0.014$  (see Table. I). The systematic uncertainty stems mostly from microwave dispersion. The largest contribution to the infidelity is spin decoherence, likely caused by the high density of defects in the crystal. Comparison with the experimental data [Figs. 3(b)–3(d)] indicates that the model slightly overestimates the impact of spin decoherence [38].

By eliminating the state preparation and measurement errors, our model estimates the fidelity of the entanglement operation itself to be  $\mathcal{F}_{\text{corr}} \sim 0.83$ . Assuming better mitigation of spectral diffusion through stringent preselection [49], better suppression of the carrier through careful locking of amplitude EOM voltage bias, no microwave crosstalk,

TABLE I. Contributions to the entangled state infidelity. Marginal errors correspond to difference in simulated fidelity between the full model and one with individual sources of error eliminated. Systematic uncertainties are dominated by unknown dispersion of microwave pulses.

Entanglement Error Source	Expected Marginal Error (%)
Local Errors	
Decoherence $T_2^a$	$10.7^{+0.5}_{-0.8}$
Microwave Pulse Errors	$1.5^{+1.6}_{-1.3}$
Two-photon events	$5.3 \pm 0.2$
Heralded state error	
Systematic detuning <sup>b</sup>	$7.5 \pm 0.6$
Interferometer phase <sup>b</sup>	$7.4 \pm 0.9$
Carrier leakage	$1.6 \pm 0.6$
Spectral diffusion	$0.3 \pm 0.1$
SiV contrast <sup>c</sup>	0.7
Total Expected	$33.0^{+1.4}_{-1.7}$
Total Observed	$29.0^{+1.8}_{-1.9}$

<sup>a</sup>Comparison with Fig. 3(b) indicates that decoherence is probably overestimated.

<sup>b</sup>Errors due to systematic detuning and optimal interferometer phase are highly correlated.

<sup>c</sup>Contribution of SiV contrast relates to residual infidelity when all other sources of error are removed from the model.

and the best previously observed spin coherence [18], an entanglement fidelity of  $\mathcal{F}_{|\Psi^+\rangle} \sim 0.95$  should be achievable, still limited by residual spin decoherence. The entanglement rate is currently limited by low detection efficiency ( $\eta = 0.04$ ) and the use of a weak coherent state as heralding state. Together, this yielded a success probability of  $6 \times 10^{-4}$  per attempt and an entanglement rate of 0.9 Hz. Ultimately this protocol can reach 25% entanglement probability using single photon sources and critically coupled cavities. Using spin-dependent phase flips in overcoupled cavities [50] close to 50% entanglement probability can be reached, resulting in an entanglement rate of 50 kHz and providing an efficient mechanism for quantum networking.

In summary, we have described a protocol to entangle quantum memories with far-detuned optical transitions and demonstrated it by entangling SiVs separated by 7.4 GHz. The protocol is inherently stable, as it relies on single photon interference in a common path, and is more resource efficient than comparable entanglement schemes which require two heralding photons. Our approach can be extended both to spatially separated qubits as well as other spectrally inhomogeneous qubits [38]. The current limits can be circumvented by using stable SiV centers in separate devices, and high entanglement fidelities are possible with previously demonstrated parameters [18]. We further note that this protocol can potentially result in very high entanglement rates with low loss modulators, more sophisticated frequency modulation schemes [51], integrated filters, and a single

photon source instead of weak coherent pulses, opening the door for a broad range of new applications in quantum networking and quantum information processing.

We recently became aware of a work [52] published after our submission that analyzes related schemes for optically entangling distinguishable CQED systems.

We thank Pavel Stroganov, Eric Bersin, Leigh Martin, and Neil Sinclair for discussions, Vikas Anant from PhotonSpot for providing SNSPDs, and Jim MacArthur for assistance with electronics. This work was supported by the NSF, Center for Ultracold Atoms, Award No. 1734011, Department of Defense Army Research Office Defense University Research Instrumentation Program, Air Force Office of Scientific Research Multidisciplinary University Research Initiatives, Office of Naval Research MURI, Army Research Lab, and a Vannevar Bush Faculty Fellowship. Devices were fabricated in the Harvard University Center for Nanoscale Systems (CNS), a member of the National Nanotechnology Coordinated Infrastructure Network (NNCI), which is supported by the National Science Foundation under NSF Award No. 1541959. M. K. B. and D. S. L. acknowledge support from an National Defense Science and Engineering Fellowship. R. R. acknowledges support from the Alexander von Humboldt Foundation and the Cluster of Excellence ‘‘Advanced Imaging of Matter’’ of the Deutsche Forschungsgemeinschaft (DFG)—EXC 2056—Project No. 390715994. B. M. and E. N. K. acknowledge that this material is based upon work supported by the National Science Foundation Graduate Research Fellowship under Grant No. DGE1745303.

D. S. L., R. R., and B. M. contributed equally to this work.

\*To whom all correspondence should be addressed  
lukin@physics.harvard.edu.

- [1] A. M. Tyryshkin, S. Tojo, J. L. Morton, H. Riemann, N. V. Abrosimov, P. Becker, H. Pohl, T. Schenkel, M. L. W. Thewalt, K. M. Itoh, and S. A. Lyon, *Nat. Mater.* **11**, 143 (2012).
- [2] D. D. Sukachev, A. Sipahigil, C. T. Nguyen, M. K. Bhaskar, R. E. Evans, F. Jelezko, and M. D. Lukin, *Phys. Rev. Lett.* **119**, 223602 (2017).
- [3] M. H. Abobeih, J. Cramer, M. A. Bakker, N. Kalb, M. Markham, D. J. Twitchen, and T. H. Taminiau, *Nat. Commun.* **9**, 2552 (2018).
- [4] C. T. Nguyen, D. D. Sukachev, M. K. Bhaskar, B. Machiels, D. S. Levonian, E. N. Knall, P. Stroganov, R. Riedinger, H. Park, M. Lončar, and M. D. Lukin, *Phys. Rev. Lett.* **123**, 183602 (2019).
- [5] C. E. Bradley, J. Randall, M. H. Abobeih, R. C. Berrevoets, M. J. Degen, M. A. Bakker, M. Markham, D. J. Twitchen, and T. H. Taminiau, *Phys. Rev. X* **9**, 031045 (2019).

- [6] K. Saeedi, S. Simmons, J. Z. Salvail, P. Dluhy, H. Riemann, N. V. Abrosimov, P. Becker, H.-J. Pohl, J. J. L. Morton, and M. L. W. Thewalt, *Science* **342**, 830 (2013).
- [7] S. R. Schofield, N. J. Curson, M. Y. Simmons, F. J. Rueß, T. Hallam, L. Oberbeck, and R. G. Clark, *Phys. Rev. Lett.* **91**, 136104 (2003).
- [8] R. E. Evans, A. Sipahigil, D. D. Sukachev, A. S. Zibrov, and M. D. Lukin, *Phys. Rev. Applied* **5**, 044010 (2016).
- [9] Y. Chen, P. S. Salter, S. Knauer, L. Weng, A. C. Frangeskou, C. J. Stephen, S. N. Ishmael, P. R. Dolan, S. Johnson, B. L. Green, G. W. Morley, M. E. Newton, J. G. Rarity, M. J. Booth, and J. M. Smith, *Nat. Photonics* **11**, 77 (2017).
- [10] P. C. Maurer, G. Kucsko, C. Latta, L. Jiang, N. Y. Yao, S. D. Bennett, F. Pastawski, D. Hunger, N. Chisholm, M. Markham, D. J. Twitchen, J. I. Cirac, and M. D. Lukin, *Science* **336**, 1283 (2012).
- [11] F. Dolde, I. Jakobi, B. Naydenov, N. Zhao, S. Pezzagna, C. Trautmann, J. Meijer, P. Neumann, F. Jelezko, and J. Wrachtrup, *Nat. Phys.* **9**, 139 (2013).
- [12] L. Petit, H. G. J. Eenink, M. Russ, W. I. L. Lawrie, N. W. Hendrickx, S. G. J. Philips, J. S. Clarke, L. M. K. Vandersypen, and M. Veldhorst, *Nature (London)* **580**, 355 (2020).
- [13] E. Rosenfeld, R. Riedinger, J. Gieseler, M. Schuetz, and M. D. Lukin, *Phys. Rev. Lett.* **126**, 250505 (2021).
- [14] H. Bernien, B. Hensen, W. Pfaff, G. Koolstra, M. S. Blok, L. Robledo, T. H. Taminiau, M. Markham, D. J. Twitchen, L. Childress, and R. Hanson, *Nature (London)* **497**, 86 (2013).
- [15] H. J. Briegel, W. Dür, J. I. Cirac, and P. Zoller, *Phys. Rev. Lett.* **81**, 5932 (1998).
- [16] H. J. Kimble, *Nature (London)* **453**, 1023 (2008).
- [17] L. Childress, J. M. Taylor, A. S. Sørensen, and M. D. Lukin, *Phys. Rev. Lett.* **96**, 070504 (2006).
- [18] M. K. Bhaskar, R. Riedinger, B. Machielse, D. S. Levonian, C. T. Nguyen, E. N. Knall, H. Park, D. Englund, M. Lončar, D. D. Sukachev, and M. D. Lukin, *Nature (London)* **580**, 60 (2020).
- [19] E. Janitz, Mihir K. Bhaskar, and Lilian Childress, *Optica* **7**, 1232 (2020).
- [20] G. Vittorini, D. Hucul, I. V. Inlek, C. Crocker, and C. Monroe, *Phys. Rev. A* **90**, 040302(R) (2014).
- [21] R. Riedinger, A. Wallucks, I. Marinković, C. Löschnauer, M. Aspelmeyer, S. Hong, and S. Gröblacher, *Nature (London)* **556**, 473 (2018).
- [22] A. M. Dibos, M. Raha, C. M. Phenicie, and J. D. Thompson, *Phys. Rev. Lett.* **120**, 243601 (2018).
- [23] Y. Chu, N. P. de Leon, B. J. Shields, B. Hausmann, R. Evans, E. Togan, M. J. Burek, M. Markham, A. Stacey, A. S. Zibrov, A. Yacoby, D. J. Twitchen, M. Loncar, H. Park, P. Maletinsky, and M. D. Lukin, *Nano Lett.* **14**, 1982 (2014).
- [24] Y. Yu, F. Ma, X. Luo, B. Jing, P. Sun, R. Fang, C. Yang, H. Liu, M. Zheng, X. Xie, W. Zhang, L. You, Z. Wang, T. Chen, Q. Zhang, X. Bao, and J. Pan, *Nature (London)* **578**, 240 (2020).
- [25] N. Maring, P. Farrera, K. Kutluer, M. Mazzera, G. Heinze, and H. Riedmatten, *Nature (London)* **551**, 485 (2017).
- [26] For a fully realized quantum network with optical emitters at visible wavelengths, frequency conversion will be required for internode entanglement. However, a scheme sans frequency conversion and with higher efficiency is desirable for intranode entanglement.
- [27] S. Ates, S. M. Ulrich, S. Reitzenstein, A. Löffler, A. Forchel, and P. Michler, *Phys. Rev. Lett.* **103**, 167402 (2009).
- [28] A. Sipahigil, K. D. Jahnke, L. J. Rogers, T. Teraji, J. Isoya, A. S. Zibrov, F. Jelezko, and M. D. Lukin, *Phys. Rev. Lett.* **113**, 113602 (2014).
- [29] R. E. Evans, M. K. Bhaskar, D. D. Sukachev, C. T. Nguyen, A. Sipahigil, M. J. Burek, B. Machielse, G. H. Zhang, A. S. Zibrov, E. Bielejec, H. Park, M. Lončar, and M. D. Lukin, *Science* **362**, 662 (2018).
- [30] B. Machielse, S. Bogdanovic, S. Meesala, S. Gauthier, M. J. Burek, G. Joe, M. Chalupnik, Y. I. Sohn, J. Holzgrafe, R. E. Evans, C. Chia, H. Atikian, M. K. Bhaskar, D. D. Sukachev, L. Shao, S. Maity, M. D. Lukin, and M. Lončar, *Phys. Rev. X* **9**, 031022 (2019).
- [31] A. C. Elitzur and L. Vaidman, *Found. Phys.* **23**, 987 (1993).
- [32] K. Nemoto, M. Trupke, S. J. Devitt, A. M. Stephens, B. Scharfenberger, K. Buczak, T. Nöbauer, M. S. Everitt, J. Schmiedmayer, and W. J. Munro, *Phys. Rev. X* **4**, 031022 (2014).
- [33] C. T. Nguyen, D. D. Sukachev, M. K. Bhaskar, B. Machielse, D. S. Levonian, E. N. Knall, P. Stroganov, C. Chia, M. J. Burek, R. Riedinger, H. Park, M. Lončar, and M. D. Lukin, *Phys. Rev. B* **100**, 165428 (2019).
- [34] K. Koshino and Y. Matsuzaki, *Phys. Rev. A* **86**, 020305(R) (2012).
- [35] The choice of initial qubit state can be arbitrary as long as both the  $|\uparrow\rangle$  and  $|\downarrow\rangle$  states are coherent and represented with equal magnitude. The relative phase of the two states merely determines the type of Bell state that is prepared.
- [36] S. D. Barrett and P. Kok, *Phys. Rev. A* **71**, 060310(R) (2005).
- [37] T. Zhong, J. M. Kindem, J. G. Bartholomew, J. Rochman, I. Craiciu, V. Verma, S. W. Nam, F. Marsili, M. D. Shaw, A. D. Beyer, and A. Faraon, *Phys. Rev. Lett.* **121**, 183603 (2018).
- [38] See Supplemental Material at <http://link.aps.org/supplemental/10.1103/PhysRevLett.128.213602> for details on a more general implementation of our entanglement scheme, and extra details on the experiment, which includes Refs. [39–46].
- [39] M. J. Burek, Y. Chu, M. S. Z. Liddy, P. Patel, J. Rochman, S. Meesala, W. Hong, Q. Quan, M. D. Lukin, and M. Lončar, *Nat. Commun.* **5**, 5718 (2014).
- [40] M. J. Burek, C. Meuwly, R. E. Evans, M. K. Bhaskar, A. Sipahigil, S. Meesala, B. Machielse, D. D. Sukachev, C. T. Nguyen, J. L. Pacheco, E. Bielejec, M. D. Lukin, and M. Lončar, *Phys. Rev. Applied* **8**, 024026 (2017).
- [41] H. A. Atikian, P. Latawiec, M. J. Burek, Y. I. Sohn, S. Meesala, N. Gravel, A. B. Kouki, and M. Lončar, *APL Photonics* **2**, 051301 (2017).
- [42] R. E. Evans, M. K. Bhaskar, D. D. Sukachev, C. T. Nguyen, A. Sipahigil, M. J. Burek, B. Machielse, G. H. Zhang, A. S. Zibrov, E. Bielejec, H. Park, M. Lončar, and M. D. Lukin, *Science* **362**, 662 (2018).
- [43] M. K. Bhaskar, R. Riedinger, B. Machielse, D. S. Levonian, C. T. Nguyen, E. N. Knall, H. Park, D. Englund, M. Lončar,

- D. D. Sukachev, and M. D. Lukin, *Nature (London)* **580**, 60 (2020).
- [44] Q. Li, M. Zhu, D. Li, Z. Zhang, Y. Wei, M. Hu, X. Zhou, and X. Tang, *Appl. Opt.* **53**, 4708 (2014).
- [45] Alexander D. White, Rahul Trivedi, Kalyan Narayanan, and Jelena Vučković, *arXiv:2108.08397*.
- [46] D. L. Hurst, K. B. Joanesarson, J. Iles-Smith, J. Mørk, and P. Kok, *Phys. Rev. Lett.* **123**, 023603 (2019).
- [47] This indicates that the cross-talk between the microwave pulses is not causing substantial decoherence, as expected from the detuning  $\omega_{ZA} - \omega_{ZB}$ .
- [48] The phase and scale is determined by comparing the prediction to the data of the  $|\uparrow\uparrow\rangle_{AB}$  state.
- [49] L. Robledo, H. Bernien, I. vanWeperen, and R. Hanson, *Phys. Rev. Lett.* **105**, 177403 (2010).
- [50] T. G. Tiecke, J. D. Thompson, N. P. de Leon, L. R. Liu, V. Vuletić, and M. D. Lukin, *Nature (London)* **508**, 241 (2014).
- [51] H. H. Lu, J. M. Lukens, N. A. Peters, O. D. Odele, D. E. Leaird, A. M. Weiner, and P. Lougovski, *Phys. Rev. Lett.* **120**, 030502 (2018).
- [52] E. Callus and P. Kok, *Phys. Rev. A* **104**, 052407 (2021).